Femtosecond Pulsed Laser Deposition of Nanostructured CdS Films

Mikel Sanz[1]*, Rebeca de Nalda[1], Jose F. Marco[1], Jesus G. Izquierdo[2], Luis Bañares[2], Marta Castillejo[1]

[1]Instituto de Química Física Rocasolano, CSIC, Serrano 119, 28006 Madrid, Spain

[2] Departamento de Química Física I, Facultad de Ciencias Químicas, Universidad

Complutense de Madrid, 28040 Madrid, Spain

* Email: mikel.sanz@iqfr.csic.es

RECEIVED DATE (to be automatically inserted after your manuscript is accepted if required according to the journal that you are submitting your paper to)

Abstract

In this work we report an investigation of the properties of nanostructured deposits obtained from femtosecond pulsed laser deposition of CdS sintered targets. Specifically, we address the effect of laser irradiation wavelength, laser fluence and substrate temperature (from 25 to 450 ºC). The composition of the deposits was characterized using X-ray photoelectron spectroscopy (XPS), their crystallinity by X-ray diffraction (XRD) and the surface morphology was studied by environmental scanning electron microscopy (ESEM) and atomic force microscopy (AFM). It has been found that the smallest nanoparticles, with an average diameter of 25 nm and a narrow size distribution, together with particulates in the range 80-120 nm, are obtained at the shortest laser wavelength of 266 nm on room temperature substrates. Deposits do not contain microscopic droplets in any of the explored conditions.

1. Introduction

Femtosecond Pulsed Laser Deposition (fs PLD) is a versatile technique for the fabrication of metal and semiconductor nanoparticles due to the possibilities it offers to control size and shape of nanodeposits by varying the laser parameters. Various studies[1-7] have shown the possibility of using fs PLD as a general route to nanoparticle formation and have demonstrated that the nature of nanostructured deposits grown by fs PLD strongly depends on the material and deposition conditions. However, the majority of these studies have been performed with light pulses centered around the peak wavelength of the Ti:Sapphire laser at 800 nm and few reports have explored the effect of this parameter. Analysis of the process over a broader range of wavelengths can provide important information about the nanoparticle formation processes and serve as experimental tests for advanced theoretical models. The wavelength dependence of nanostructured films produced by fs PLD has been studied for ZnO,[8] Si,[9] Ni[10] and TiO_2[11] and an increase of characteristic sizes with wavelength has been reported. In PLD of semiconductors, the excitation laser wavelength plays an important role related with the energy band gap. A recent work has demonstrated the influence of wavelength in fs PLD of TiO_2 on the control of the nanoparticle size and on the reduction of microparticulates.[11]

CdS is well known as a very important II-VI compound semiconductor material for the development of various modern technologies such as solar cells, light emitting diodes, laser heterostructures, photoconductors, optical waveguides and switches, nonlinear integrated optical devices, etc.[12] CdS nanoparticles and nanostructures have been produced using different methods including chemical colloidal synthesis, sol-gel, electrochemical deposition, Langmuir-Blodget, sputtering, molecular beam epitaxy, etc.[12] In particular, PLD has served to fabricate nanostructured CdS films using pulses of both nanosecond (ns)[13-19] and fs[20-22] duration. In the case of ns PLD, intensive studies of the features of the deposits as a function of pulse laser duration and wavelength have been performed (see for example Ref. 14 and references therein). However, the dependence of the fs PLD nanostructured films on laser

3

fluence,[20] substrate material and temperature[21,22] has been characterized only at the laser wavelength of 800 nm.

In this work, CdS nanostructured deposits have been grown on Si (100) substrates by laser ablating a CdS sintered target in vacuum using a Ti:Sapphire laser delivering 60 fs pulses. The effect of the laser irradiation wavelength on the obtained nanostructures is investigated using 266, 400 and 800 nm in a range of conditions that are suitable for obtaining nanostructured films. The influence of laser fluence and substrate temperature was also studied. Results are discussed in reference to the crystalline quality and composition of the deposits, characterized using X-ray diffraction (XRD) and X-ray photoelectron spectroscopy (XPS) respectively, and to the surface morphology, as monitored by environmental scanning electron microscopy (ESEM) and atomic force microscopy (AFM).

2. Experimental

The experimental set up consists of a PLD stainless steel chamber evacuated by a turbomolecular pump down to 2×10^{-4} Pa. CdS targets were prepared from CdS powder (Alfa Aesar 99.999%) that was pelletized into disks of 10 mm diameter and about 2 mm of thickness using a hydrostatic press at 8 Ton/cm^2 followed by sintering at 350 °C in air for 12 h. Targets were placed on a rotating sample holder to avoid crater formation by repetitive laser irradiation. Pulses of 60 fs were produced by a Ti:Sapphire amplified laser system (Spectra Physics) centered at 800 nm operating at a repetition rate of 1 kHz. Shorter radiation wavelength at 400 and 266 nm was generated by using a BBO based frequency doubler/tripler. The temporal profile of the 800 nm pulses was diagnosed with a second harmonic generator autocorrelator. Energy control was performed by a half-wave plate/polarizer combination. The laser beam was focused onto the target with a 25 cm focal length lens at 35º with different fluences. The Si (100) substrates were ultrasonically degreased in acetone and methanol for 10 min. They were mounted on a heating element that allowed operation in the temperature range between 25 and 450º C and placed at a distance of 4 cm in front of the target. Deposits were grown in all cases with 6×10^5 pulses.

The modification of the irradiated area of the targets was studied by optical microscopy (Leica, S8APO) with a 160 x microscope objective and equipped with a CCD camera. The influence of the deposition conditions on the crystallinity of the deposits was studied by XRD (Philips XPert) using Cu Kα (1.54 Å) radiation in the θ/2θ configuration. The deposits were also analyzed by XPS using a Leybold LHS-10 XPS spectrometer, under an operating vacuum better than 1×10^{-6} Pa, using Mg Kα radiation (130 W) and an analyzer transmission energy of 200 and 20 eV for the wide and narrow scan spectra respectively. The spectra were recorded at take-off angles of 90º. All binding energy (BE) values were charge-corrected to the adventitious C 1s signal which was set at 284.6 eV and are accurate to ± 0.2 eV. Relative atomic concentrations were calculated using tabulated atomic sensitivity factors.[23] The surface morphology of the deposits was examined by ESEM (Philips XL30) and by AFM (Digital Instruments). All the AFM images were obtained in tapping mode and they were post-processed using a second-order flattening routine. Film thickness was measured by AFM.

3. Results and Discusion

3.1 Ablation thresholds

For short pulse regime, the modification threshold fluence F_{th} depends on the material and the number of laser pulses applied to the same spot.[24] This incubation effect is attributed to surface defects generated by irradiation with multiple laser pulses that lead to changes in mechanical and/or chemical properties of the material and induce a reduction of the threshold with the number of pulses. In the condition of fabrication of deposits, it was estimated that around 50 laser pulses were applied to the same position of the target. Therefore, in order to obtain deposits under comparable conditions for the different laser wavelengths, ablation of targets was performed at laser fluences of 1.5 and 3.5 times the threshold at this number of pulses for the three wavelengths and also at 5 times the threshold for 266 and 800 nm (at 25 ºC). To determine these fluence thresholds we studied the surface modifications generated at different laser fluences using the spot regresion method.[25] Briefly, when laser pulses posses a Gaussian spatial beam profile, the laser fluence, F, on the sample surface and the diameter D of the

modified area are related by $D^2 = 2\omega_0 \ln (F/F_{th})$, where ω_0 is the $1/e^2$ radius of the beam intensity distribution and the fluence is related to the pulse energy by $F = E/\pi\omega_0^2$. From a plot of the D^2 versus lnE, F_{th} can be determined. By aplying this method, the resulting thresholds are 40, 55, and 260 mJ/cm^2, with around 10 % error, for 266, 400 and 800 nm, respectively. The beam size in the focal position was similar for the three wavelengths, with a value of $\omega_0 = 50 \pm 10$ μm. While thresholds measured at 400 and 266 nm are similar, the threshold at 800 nm is around 5 times higher. This difference is related with the order of the absorption procces that sends the electron to the conduction band of the semiconductor. The energy band gap of CdS is 2.42 eV,[12] which corresponds to 512 nm. One photon (i. e. a linear process) at either 266 or 400 nm radiation is enough to promote the electron to the conduction band whereas at 800 nm a mechanism of multiphoton nature (involving two photon absorption) would be required. A similar tendency of fluence threshold with wavelength was observed in TiO$_2$[11] whose band gap is 3.0 eV.

3.2 Composition

XPS spectra of the obtained deposits were recorded to determine their stoichiometry. All Cd 3d and S 2p spectra from the different samples were essentially identical (typical examples are given in Figure 1a and 1b, respectively). The binding energy of Cd 3d$_{5/2}$ core level was 405.2 ± 0.2 eV in all cases and that of S 2p$_{3/2}$ core level was 161.1 ± 0.2 eV. These values are fully compatible with the presence of CdS.[26] The quantitative analysis revealed a fully stoichiometric ratio in deposits grown at 266 nm, 25 ºC. At all other conditions of deposition (irradiation wavelength of 400 and 800 nm and substrate temperatures higher than 25º C) a higher Cd/S atomic ratio than expected is obtained. These measured ratios vary from 1.0 to 1.5; however, no clear trend with either wavelength or substrate temperature has been found. Since the samples are richer in Cd, this suggests that, most probably, they contain a noticeable proportion of metallic Cd. A previous study performed at 800 nm[22] has reported a richer content of cadmium in the deposited film as the substrate temperature increases, which has been attributed to enhanced evaporation of sulfur from the film as the temperature increases.

3.3 Surface crystallinity

Figure 2 presents the θ/2θ XRD patterns of films obtained by ablation at 266 and 800 nm at various fluences. They present broad and weak diffraction peaks indicating that the obtained CdS films consist of a mixture of crystalline and amorphous phases. The XRD peaks are located at 25.1º, 26.6º, 28.2º, 36.6º, 43.9º, 47.9º and 52.1º and are assigned to CdS (100), CdS (002), CdS (101), CdS (102), CdS (110), CdS (103) and CdS (112), respectively. This pattern reveals the predominance of the hexagonal (wurtzite) polycrystalline structure of CdS (Joint Committee on Powder Diffraction Standards Card No. 77-2306). The diffraction peak observed at ~ 30º corresponds to Si (200) and probably it is due to multiple scattering effects from spots in higher-order Laue zones close to the Ewald sphere.

In this type of crystalline structure, the perpendicular orientation of the *c*-axis with respect to the substrate surface is indicated by the dominating appearance of the CdS (002) peak. A weak CdS (002) peak and intense CdS (100) and CdS (110) peaks indicate a parallel orientation of the *c*-axis.[14] The XRD results show that the deposited material present a mixture of the two orientations. This could be explained by a sudden solidification of the material on the substrate which prevents the slower growth on a preferential direction.[22] It has been observed that a longer wavelength (Figure 2a) and a higher fluence (Figure 2b) favor the perpendicular orientation, as shown by the predominance of the CdS (002) phase. This dependence indicates that the nucleation processes that take place in the substrate are not the only factor governing the final characteristics of the deposited structures, and that some control can be exerted on the crystallinity through changes in the laser-target interaction.

3.4 Surface structure

The superficial structure of deposits was measured by ESEM and AFM and, as observed in Figures 3 and 4, the nanostructured films mainly contain nanoparticles smaller than 50 nm and few larger particulates with sizes ranging from 80 to 300 nm. Determined dimensions are summarized in Table 1. The film thickness varies from 30 nm, for a sample prepared at the wavelength of 266 nm at the lowest

used fluence (1.5 times the threshold), to 200 nm measured in a sample grown at the wavelength of 800 nm and the highest used fluence (5 times the threshold).

The size and density of the larger particulates were analyzed by ESEM. Figure 3 shows images of deposits obtained at 25 ºC. At 266 nm (Figure 3a), a layer of low superficial density (45 μm^{-2}) of small particulates (with sizes in the range 80-120 nm) is present. The particulate size and density increase with substrate temperature as observed in Table 1. This result is related with the mobility of the deposited material on the surface, which is favored by increasing the substrate temperature. By operating at 400 nm (Figure 3b), a somewhat higher number of particulates is obtained whereas at 800 nm (Figure 3c) the number of particulates with larger sizes increases considerably. It was also noted that in the range of laser fluences used to obtain the deposits (1.5 and 5 times the modification threshold) changes in the size of particulates are not observed, although their density decreases with fluence, an effect possibly related with the more extensive degree of fragmentation in the plume as the laser pulse energy is increased.

The surface morphology and topography were investigated in greater detail by AFM to characterize the deposited nanoparticles. As an example, Figure 4 shows images of deposits grown by PLD at 266 nm at different substrate temperatures. The increase in the average size of nanoparticles with increasing temperature is clear. Their diameters have been measured from the profiles of the topographical AFM images recorded with the Scanning Probe Microscopy software WSxM (Nanotec). Figure 5 presents the size histograms together with the corresponding log-normal fitting, $Y = Y_0 + A\ exp[-2(X-X_c)^2/\ w^2]/\ w(\pi/2)^{1/2}$ with the fitting parameters Y_0 = offset, A = amplitude, X_c = center and w = width. The average diameter of the nanoparticles was obtained from the X_c parameter of the fitting. At 25 ºC a high density of nanoparticles (530 μm^{-2}) with a narrow size distribution is observed, with average diameters of 26 ± 1 nm and absence of particulates larger than 100 nm (Figure 4a). Upon heating of the substrate, the obtained size distribution of nanoparticles becomes broader and the average diameter increases slightly with temperature to 51 ± 3 nm at 450 ºC (Figure 4d). A similar analysis was performed for 400 and 800 nm irradiation. At 400 nm (Figure 4e) the size of nanoparticles is similar to that measured at 266 nm at

the same temperatures. At 800 nm (Figure 4f), larger nanoparticles and some larger particulates are also observed (Table 1). Therefore, of all explored conditions, the smallest nanoparticles (with average diameter 26 nm), highest nanoparticle density and the narrowest size distribution were obtained by ablation at 266 nm at 25 ºC.

The results clearly show that the wavelength of the laser used for deposition has a strong effect on the characteristics of the nanoparticles produced by fs PLD. The tendency of producing smaller nanoparticles with a narrower size distribution at shorter wavelengths as observed herein has also been reported before[8-11] and discussed in terms of the larger strain rate in the expansion of the plasma fluid into vacuum following irradiation of the target by UV pulses.[10] In fact, at the laser wavelengths of this study, the linear absorption coefficients of the target are $\alpha_{266} \approx 8 \times 10^5$ cm^{-1}, $\alpha_{400} \approx 1.5 \times 10^5$ cm^{-1} and $\alpha_{800} \approx 10^4$ cm^{-1}.[27,28] Upon 266 nm irradiation, and due to the high absorption coefficient, a layer of only around 12 nm below the surface of the target is heated up as irradiation of the target by the pulse proceeds, whereas this penetration depth is 66 and 1000 nm for excitation wavelengths of 400 and 800 nm, respectively. Therefore, the experimentally observed tendency of producing smaller nanoparticles at 266 nm irradiation can be assigned to the smaller fragments produced due to the larger strains induced in a reduced volume during the relaxation of ablated CdS. The heat diffusion time is defined as $\tau_d = 1/\alpha^2 D_h$, with $D_h = 0.1$ cm^2 s^{-1} the heat diffusion coefficient of CdS.[29] Even at the shortest wavelength (266 nm), which corresponds to the highest absorption coefficient, the duration of the laser pulse is shorter than the heat diffusion time, of around 10 ps. This diffusion time increases significantly at 400 and 800 nm irradiation. In the short time of the laser pulse duration, thermal equilibrium between the electrons and the lattice is not achieved and the ablated material does not have time to expand before the end of the pulse. In this process, once energy deposition is complete, the plasma expands adiabatically from an initially high temperature. As the plasma reaches densities close to the critical point in the phase diagram, phase decomposition takes place with high fragmentation leading to the observed small nanoparticle formation.

The observed trend of producing smaller nanoparticles with a narrower size distribution at shorter wavelengths of the fs laser can also be discussed in the framework of the thermodynamic analysis method developed by Lewis and Perez.[3] According to this model, ablation mechanisms, operating under fs irradiation of strongly absorbing targets, can be related with the depth of the affected region below the surface of the target, which in turn determines the trajectory followed by the material in the phase diagram. Upon irradiation at short wavelength, the superficially affected region of the material is exposed to an intense heating rate that decomposes the solid by exceeding its cohesive energy: This finally results in its complete vaporization and therefore favors the generation of small size nanoparticles. When longer irradiation wavelengths are used, deeper regions of the target are affected; in this case phase explosion and fragmentation are the dominant mechanisms which lead to a more inhomogeneous mixture of larger size fragments as observed herein.

The results of this work provide a good experimental test for advanced theoretical models of fs laser ablation and exemplify the possibility of exerting control of the dimensions and crystalline properties of nanodeposits by varying the laser wavelength. More work is in progress to further confirm the observed dependence by using other wavelengths in a broader range of semiconducting targets.

4. Conclusions

CdS nanostructured deposits on Si (100) substrates were obtained from sintered CdS targets at the wavelengths of 266, 400 and 800 nm from a fs Ti:Sapphire laser. The deposits consist of CdS nanoparticles with grain size down to 25 nm with overimposed larger particles in the 80 to 300 nm range. The obtained deposits are almost stoichiometric and the preferential orientation of the crystallites with respect to the substrate surface can be tuned by changing the laser fluence and wavelength. The most uniform deposits, showing the highest density of nanoparticles of around 25 nm diameter, were grown by ablation at 266 nm in vacuum at 25 ºC. The highest concentrations of particulates and largest nanoparticles were observed at the longest laser wavelengths, 800 nm. The observed trend of size reduction of deposited nanostructures as the laser wavelength decreases, and the importance of this

parameter in the crystalline properties of the deposits, provide important clues about the processes of formation of nanoparticles, giving the possibility of tailoring the properties of nanoparticles formed by fs PLD.

References

[1] Chichkov, B.N.; Momma, C.; Nolte, S.; von Alvensleben, F.; Tünnermann, A. *Appl. Phys. A* **1996**, *63,* 109.

[2] Perrière, J.; Millon, E.; Chamarro, M.; Morcrette, M.; Andreazza, C. *Appl. Phys. Lett.* **2001,** *78,* 2949.

[3] Lewis, L.J.; Perez, D. *Appl. Surf. Sci.* **2009,** *255*, 5101.

[4] Eliezer, S.; Eliaz, N.; Grossman, E.; Fisher, D.; Gouzman, I.; Henis, Z.; Pecker, S.; Horovitz, Y.; Fraenkel, M.; Maman, S.; Lereah, Y. *Phys. Rev. B* **2004,** *69,* 144119.

[5] Amoruso, S.; Ausanio, G.; Bruzzese, R.; Vitiello, M.; Wang, X. *Phys. Rev. B* 2005*, 71*, 033406.

[6] Zhang, Y.; Russo, R.E.; Mao, S.S. *Appl. Phys. Lett.* **2005,** *87*, 133115.

[7] Perrière, J.; Boulmer-Leborgne, C.; Benzerga, R.; Tricot, S. *J. Phys. D: Appl. Phys.* **2007,** *40*, 7069.

[8] Okoshi, M.; Higashikawa, K.; Hanabusa, M. *Jpn. J. Appl. Phys.* **2001,** *40,* 1287.

[9] Amoruso, S.; Bruzzese, R.; Spinelli, N.; Velotta, R.; Vitiello, M.; Wang, X.; Ausanio, G.; Iannotti, V.; Lanotte, L. *Appl. Phys. Lett.* **2004,** *84,* 4502.

[10] Amoruso, S.; Ausanio, G.; Barone, A.C.; Bruzzese, R.; Campana, C.; Wang, X. *Appl. Surf. Sci.* **2007,** *254,* 1012.

[11] Sanz, M.; Walczak, M.; DeNalda, R.; Oujja, M.; Marco, J.F.; Rodríguez, J.; Izquierdo, J.G.; Bañares, L.; Castillejo, M. *Appl. Surf. Sci.* **2009,** *255*, 5206.

[12] Hullavarad, N.V.; Hullavarad, S.S.; Karulkar, P.C. *J. Nanoscie. Nanotech.* **2008,** *8*, 3272.

[13] Keitoku, S.; Ezumi, H. *Sol. Energy Mater. Sol. Cells* **1994,** *35,* 299.

[14] Ullrich, B.; Sakai, H; Segawa, Y. *Thin Solid Films* **2001,** *385,* 220.

[15] Perna, G.; Capozzi, V.; Ambrico, M.; Augelli, V.; Lingonzo, T.; Minafra, A.; Schiavulli, L.; Pallara, M. *Thin Solid Films* **2004,** *187,* 453.

[16] Mahdavi, S.M.; Iraji zad, A.; Tilaki, R.M. *Optical Materials* **2005,** *27*, 1583.

[17] Vigil-Galán, O.; Vidal-Larramendi, J.; Escamilla-Esquivel, A.; Contreras-Puente1, G.; Cruz-Gandarilla, F.; Arriaga-Mejía, G.; Chavarría-Castañeda, M.; Tufiño-Velázquez, M. *Phys. Stat. Sol.* **2006,** *203,* 2018.

[18] Acharya, K.P.; Skuza, J.R.; Lukaszew, R.A.; Liyanage, C.; Ullrich, B. *J. Phys.: Condens. Matter* **2007,** *19,* 196221.

[19] El Deeb, A.F. *Eur. Phys. J. Appl. Phys.* **2007,** 38, 252.

[20] Tong, X.L.; Jiang, D.S.; Liu, L.; Liu, Z.M.; Luo, M.Z. *Opt. Comm.* **2007,** *270*, 356.

[21] Tong, X.L.; Jiang, D.S.; Li, Y.; Liu, Z.M.; Luo, M.Z. *Physica B* **2006,** *382,* 105.

[22] Tong, X.L.; Jiang, D.S.; Liu, Z.M.; Luo, M.Z.; Li, Y.; Lu, P.X.; Yang, G.; Long, H. *Thin Solid Films* **2008,** *516,* 2003.

[23] Wagner, C.D.; Davis, L.E.; Zeller, M.V.; Taylor, J.A.; Raymond, R.M.; Gale, L.H. *Surf. Interface Anal.* **1981,** *3,* 211.

[24] Baudach, S;Bonse, J.; Kautek, W. *Appl. Phys. A* **1999,** *69,* S395.

[25] Jandeleit, J.; Urbasch, G.; Hoffmann, H.; Treusch, H.G.; Kreutz, E. *Appl. Phys. A* **1996,** *63*, 117.

[26] Marychurch, M.; Morris, G.C. *Surf. Sci.* **1985,** *154,* L251.

[27] Gottesman, J.; Ferguson, W.F.C. *J. Opt. Soc. Am.* **1954,** *44*, 368.

[28] Ninomiya, S.; Adachi, S. *J. Appl. Phys.* **1995,** *78*, 1183.

[29] Thoma, M.L.; Weber, C.; Klingshirn, C. *Appl. Phys. A* **1991,** *52*, 255.

Table 1. Composition and dimensions of nanostructured CdS deposits.

wavelength (nm)	substrate temperature (ºC)	size range of particulates (nm)	density of particulates (μm^{-2})	average size of nanoparticles (nm)	density of nanoparticles (μm^{-2})
	25	80-120	45	26	530
	150	80-120	60	31	400
266	350	100-140	76	36	360
	450	120-160	80	51	280
400	25	80-140	64	30	510
800	25	150-300	80	54	200

Figure Captions

Figure 1. XPS spectra of deposits grown at 266 nm heating the substrate at 350 ºC: a) Cd 3d spectrum and b) S 2p spectrum.

Figure 2. XRD patterns of films deposited at 25 ºC: a) at fluence of 5 F_{th} at 266 and 800 nm, and b) at fluence of 1.5 F_{th} and 5 F_{th} at 266 nm.

Figure 3. ESEM images of the surfaces of CdS nanostructured films grown at 25 ºC at: a) 266 nm, b) 400 nm and c) 800 nm.

Figure 4. AFM topography images (1 x 1 μm^2) of the nanostructures deposited at 266 nm at substrate temperature of: a) 25 ºC, b) 150 ºC, c) 350 ºC and d) 450 ºC and at 25 ºC and at: e) 400 nm and f) 800 nm.

Figure 5. Size histograms of the nanoparticles produced by laser ablation at 266 nm and substrate temperature of: a) 25 ºC, b) 150 ºC, c) 350 ºC and d) 450 ºC and at 25 ºC and at: e) 400 nm and f) 800 nm. Lines correspond to the log-normal fitting.
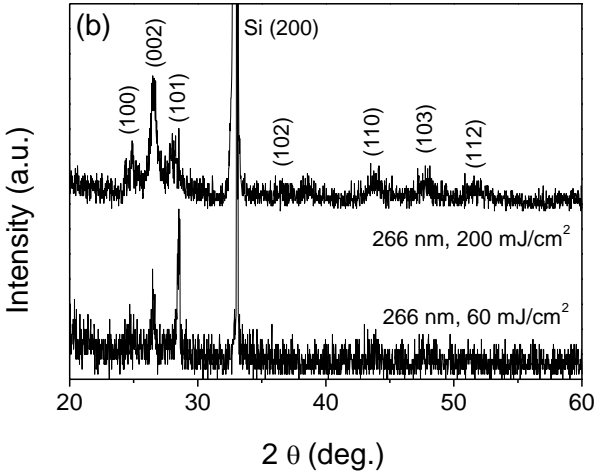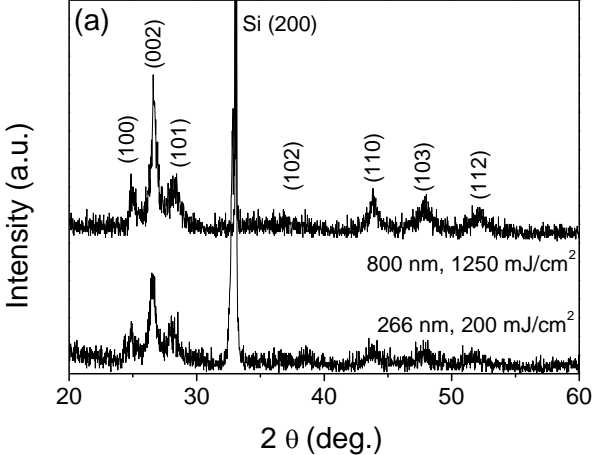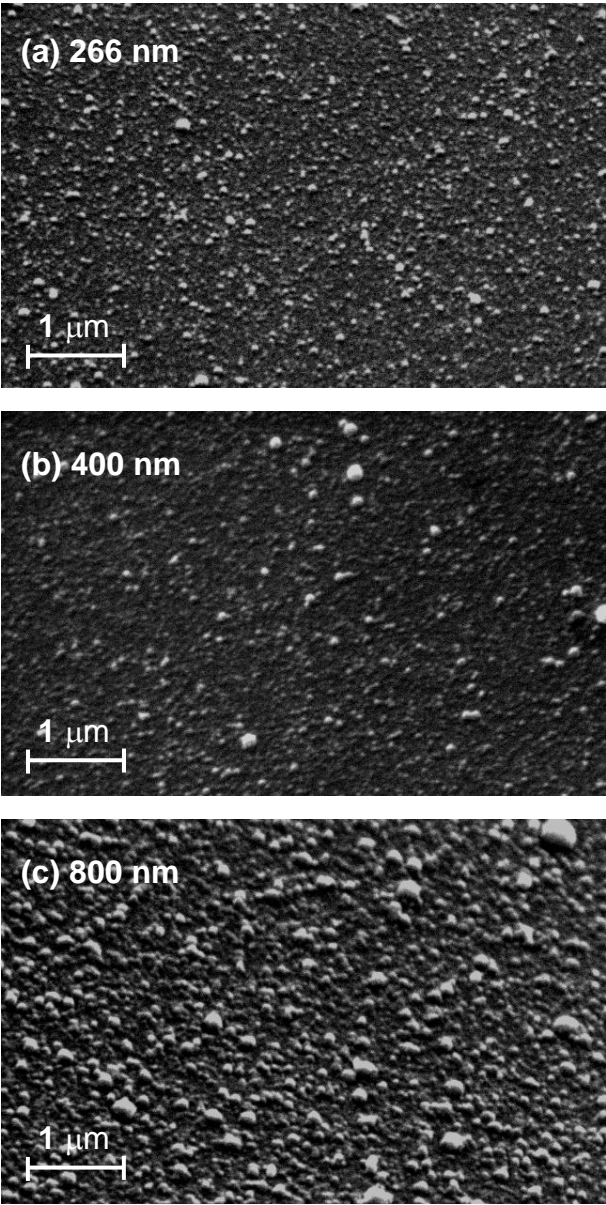
Figure 1

Figure 2

Figure 3

(a) 266 nm

1 μm

(b) 400 nm

1 μm

(c) 800 nm

1 μm

Figure 4

Figure 5

Relative frequency

(a) 266nm 25 ºC

(b) 266nm 150 ºC

(c) 266nm 350 ºC

(d) 266nm 450 ºC
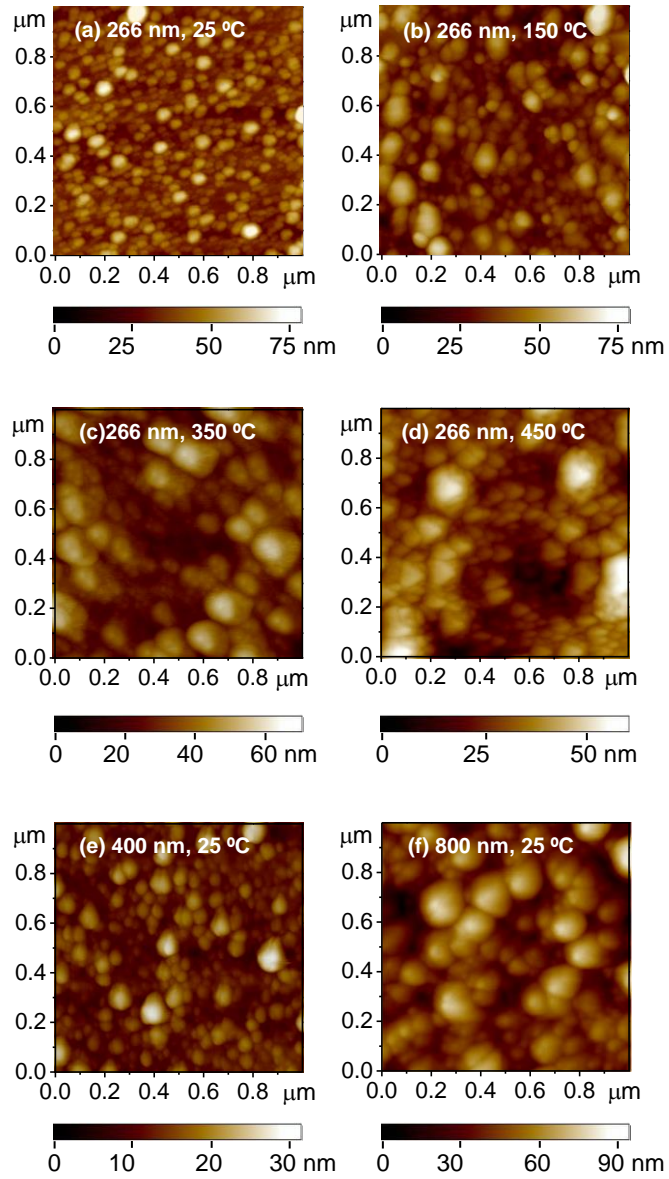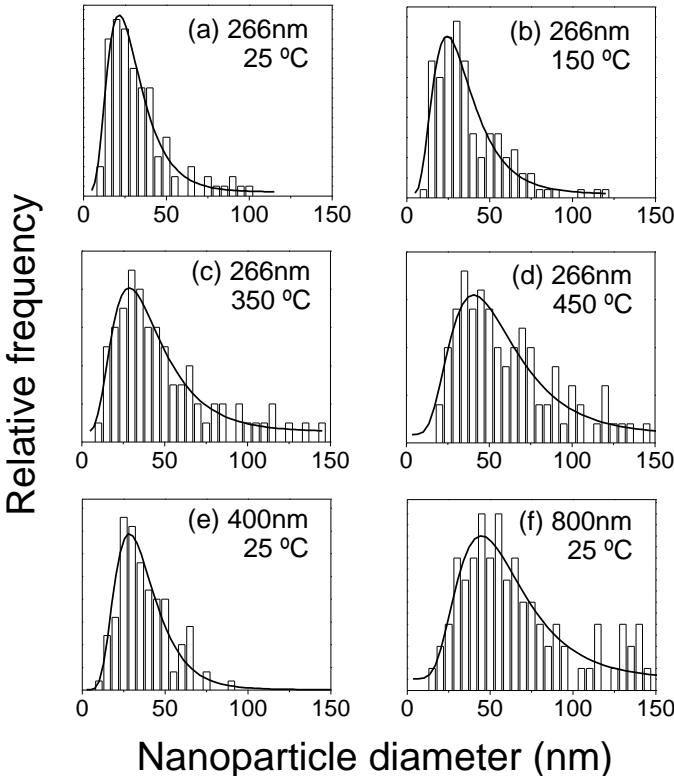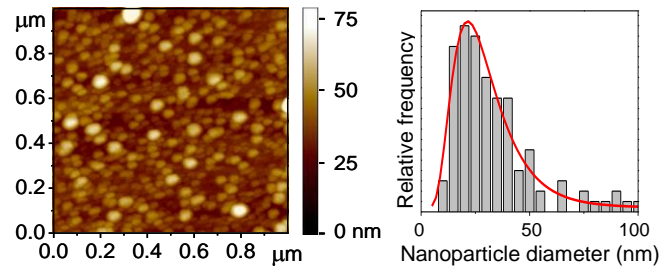
(e) 400nm 25 ºC

(f) 800nm 25 ºC

Nanoparticle diameter (nm)
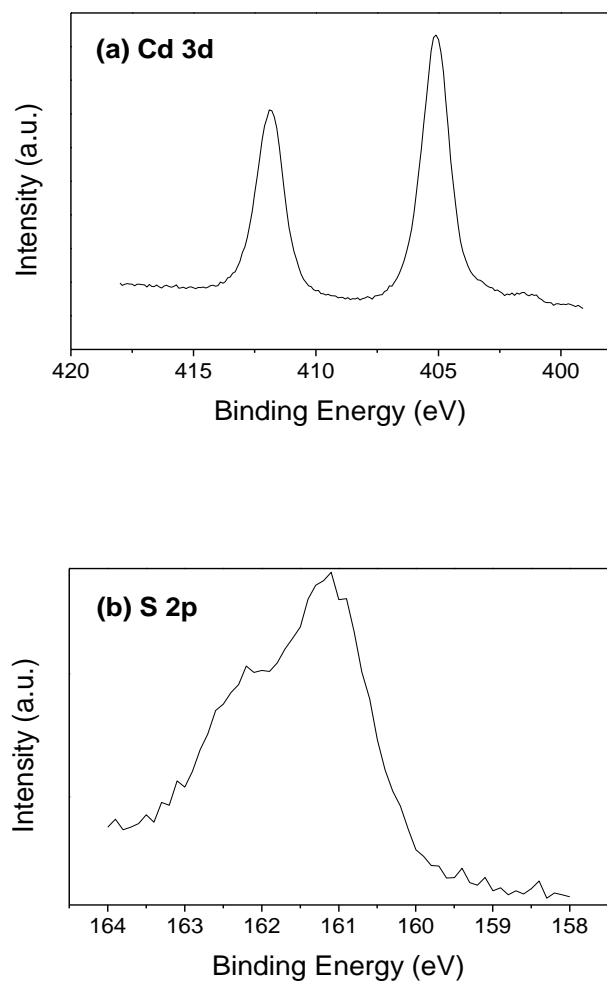
"Table of Contents" graphic

Graphic caption: AFM topography and size histogram of the nanostructures deposited at 266 nm at substrate temperature of 25 ºC.